

MICROWAVE EMISSION FROM SPINNING DUST IN CIRCUMSTELLAR DISKS

ROMAN R. RAFIKOV^{1,2}

Received 2006 February 1; accepted 2006 March 30

ABSTRACT

In the high-density environments of circumstellar disks dust grains are expected to grow to large sizes by coagulation. Somewhat unexpectedly, recent near-IR observations of PAH features from disks around Herbig Ae/Be stars demonstrate that a substantial amount of dust mass in the surface layers of these disks (up to several tens of percent of the local carbon content) can be locked up in small nanometer-sized particles. We investigate the possibility of detecting the electric dipole emission produced by these nanoparticles (sizes ~ 1 nm) as they spin at thermal rates (tens of GHz) in cold gas. We show that such emission peaks in the microwave range and dominates over the thermal disk emission at $\nu \lesssim 50$ GHz typically by a factor of several if $\gtrsim 5\%$ of the total carbon abundance is locked up in nanoparticles. We test the sensitivity of this prediction to various stellar and disk parameters and show that if the potential contamination of the spinning dust component by the free-free and/or synchrotron emission can be removed, then the best chances of detecting this emission would be in disks with small opacities, having SEDs with steep submillimeter slopes (which minimize thermal disk emission at GHz frequencies). Detection of the spinning dust emission would provide important evidence for the existence, properties, and origin of the population of small dust particles in protoplanetary disks, with possible ramifications for planet formation.

Subject headings: accretion, accretion disks — circumstellar matter — dust, extinction — stars: pre-main-sequence

Online material: color figures

1. INTRODUCTION

Recent IR and submillimeter observations of disks around young stars strongly support the idea that dust grains in these disks are significantly evolved compared to their interstellar medium (ISM) counterparts. There is mounting evidence that in many young stellar systems dust grains have sizes reaching centimeters (Testi et al. 2003; Acke et al. 2004; Natta et al. 2004), in contrast to the submicron sizes of the ISM dust particles, which is a natural consequence of grain growth by coagulation. This process is often accompanied by a change of the material properties of dust grains indicated by their increased crystallinity (van Boekel et al. 2005) and by settling of dust toward the disk mid-plane inferred from the change of the shape of the spectral energy distribution (SED) of disks (Acke et al. 2004). Observational evidence for dust growth exists not only in protoplanetary disks around T Tauri stars (stellar mass $M_* \lesssim 2 M_\odot$), but also in their analogs around higher mass ($2 M_\odot \lesssim M_* \lesssim 10 M_\odot$) Herbig Ae/Be stars (van Kerckhoven et al. 2002; Sloan et al. 2005; Schütz et al. 2005; Habart et al. 2005), as well as in disks around substellar objects (Apai et al. 2005).

At the same time, recent observations of the polycyclic aromatic hydrocarbon (PAH) spectral features in disks of Herbig Ae/Be stars (Meeus et al. 2001; Acke & van den Ancker 2004) provide evidence for the presence of very small dust grains (sizes $a \sim 3-100$ Å) in these disks. Previously, the existence of a significant amount of carbonaceous nanoparticles in the ISM has been proposed to explain the *IRAS* (*Infrared Astronomical Satellite*) observations of “unidentified infrared” emission features and a strong mid-infrared emission component resulting from the starlight reprocessing by the ultrasmall grains (Boulanger & Pérault 1988). The proposed fraction of the ISM carbon mass locked up

in very small grains considerably exceeds that implied by the extension of the conventional MRN (Mathis-Rumpl-Nordsieck) dust size distribution (Mathis et al. 1977) to very small sizes, below 50 Å. This suggests the existence of a separate population of very small carbonaceous grains that is distinct from the MRN distribution and contains $\sim 10\%$ of the C in the ISM (Leger & Puget 1984; Draine & Anderson 1985). Thus, it is not surprising that nanoscale dust particles should exist at some level in disks³ around Herbig Ae/Be stars, since the latter were originally part of the ISM. However, the detailed modeling of the IR emission features in these systems suggests that PAHs may contain as much as several tens of percent of the total C mass in disks (Habart et al. 2004), provided that all dust grains are fully mixed in the vertical direction. These results could be interpreted as indicating that the small-dust population in these disks does not only withstand coagulation, but on the contrary may have gained some additional mass, presumably due to the fragmentation of larger particles. This suggests a very interesting size-dependent evolution of the dust population in Herbig Ae/Be disks. In the case of disks around T Tauri stars and brown dwarfs it is difficult to make definite statements about the presence of small dust grains (although see Geers et al. 2005) because of the lack of strong stellar UV fluxes needed for exciting PAH molecules (see Li & Draine 2002; Smith et al. 2004 for an alternative view).

In this paper we describe a new observational channel for probing the presence and properties of very small dust grains in disks around young stellar objects. In the outer parts of these disks, $\sim 10^2$ AU from the central star, nanometer-sized dust particles spin at thermal rates of several tens of GHz. Because of their intrinsic dipole moments, these “macromolecules” emit electric dipole radiation in the microwave band, where the thermal

¹ Canadian Institute for Theoretical Astrophysics (CITA), McLennan Physics Labs, 60 St. George Street, University of Toronto, Toronto ON M5S 3H8 Canada; rrr@cita.utoronto.ca.

² Canada Research Chair.

³ A possible origin of observed PAH emission in the roughly spherical envelopes around stars rather than in disks is unlikely given the correlation between the strength of the PAH emission and the disk geometry inferred from the SED shape (Habart et al. 2004).

Rayleigh-Jeans emission of the circumstellar disk is rather weak. This makes it possible to disentangle the spinning dust contribution to the disk emission and study the properties of this dust component. We describe the physics of the spinning dust emission and analyze its observational signatures in § 2. Applications of our results are discussed in § 3.

2. EMISSION FROM SPINNING DUST GRAINS

Ferrara & Dettmar (1994) proposed that charged ISM dust grains spinning at thermal rates can produce observable microwave emission via electric dipole radiation. This mechanism has been further investigated in detail by Draine & Lazarian (1998b, hereafter DL98), who considered, among other things, intrinsic dipole moments of grains, various processes governing the non-thermal spin rates of grains, and a size distribution of emitting nanoscale particles consistent with previous detections of PAH emission from the ISM. In this paper we largely follow the approach adopted in these pioneering investigations.

2.1. Circumstellar Disk Model

We describe the structure of the circumstellar disk using the conventional two-temperature flared disk model of Chiang & Goldreich (1997), which states that the vertical extent of the disk can be split into two well-defined regions: an upper “exposed layer,” in which dust absorbs most of the incoming starlight and reradiates it in the infrared, and a lower “shielded region,” which is hidden from direct starlight and is warmed only by the reprocessed radiation of the outer layer. For our purposes both layers can be considered isothermal with different temperatures. The temperature of the shielded layer T_{sh} is lower than that of the overlying exposed layer by a factor of several.

The amount of mass contained in the exposed layer is very small: the fraction of the total disk surface density Σ corresponding to this layer is $\sim \gamma / [\kappa_{\text{p}}(T_{\star})\Sigma]$, where $\gamma \lesssim 0.1$ is the disk flaring angle and $\kappa_{\text{p}}(T_{\star})$ is the Planck opacity at the stellar temperature. Since it is likely that even in the distant parts of the disk $\kappa_{\text{p}}(T_{\star})\Sigma \gg 1$, the shielded region must contain most of the disk mass. Thus, if small particles are well mixed throughout the disk (which is a reasonable assumption for very small grains having settling times longer than the disk lifetime), most of the small dust particles must be shielded from the direct stellar illumination by the outer exposed layer. This inference significantly simplifies our subsequent treatment.

We assume a simple power-law profile for the disk surface density,

$$\Sigma(r) = \Sigma_1 r_1^{-\alpha}, \quad (1)$$

where r_1 is the distance from the star normalized by 1 AU, Σ_1 is the surface density at 1 AU, and α is a parameter that we can vary. The midplane temperature profile $T_{\text{sh}}(r)$ needed for the calculation of the grain spin rates is computed in the Appendix according to the prescription of the flared disk model of Chiang & Goldreich (1997).

At the low temperatures of interest for us, the opacity κ_{ν} is due to dust grains. At long wavelengths κ_{ν} typically scales as a power law of ν , and we adopt in this study (following the notation of Beckwith et al. 1990)

$$\kappa_{\nu} = \kappa_{12} \nu_{12}^{\beta}, \quad (2)$$

where $\nu_{12} = \nu / (10^{12} \text{ Hz})$ is the radiation frequency normalized by 10^{12} Hz and κ_{12} is the opacity at 10^{12} Hz . The power-law index β can be directly measured from the disk SED in the

submillimeter range, and in protoplanetary disks it varies from 0.3 to 1.5 (Kitamura et al. 2002), while ISM emission is characterized by $\beta \approx 1.7$ (Finkbeiner et al. 1999). Small values of β in protoplanetary disks are interpreted as the evidence for grain growth (Natta et al. 2004; Draine 2006).

The normalization of the opacity at a given frequency κ_{12} is rather poorly constrained. Beckwith et al. (1990) advocate using $\kappa_{12} = 0.1 \text{ cm}^2 \text{ g}^{-1}$, while Kramer et al. (1998) find $\kappa(1.2 \text{ mm}) \approx 0.004 \text{ cm}^2 \text{ g}^{-1}$, which translates into $\kappa_{12} \approx 0.016 \text{ cm}^2 \text{ g}^{-1}$ for $\beta = 1$. Draine (2006) modeled absorbing properties of evolved dust populations composed of different materials with MRN size distributions extending to a maximum size $a_{\text{max}} \sim 1\text{--}10 \text{ cm}$ and found $\beta \approx 1\text{--}1.5$ and $\kappa_{12} \sim 0.01\text{--}0.1 \text{ cm}^2 \text{ g}^{-1}$ (for the dust-to-gas ratio 10^{-2}). Thus, there is at least an order-of-magnitude spread in the possible values of κ_{12} .

2.2. Spinning Dust Emissivity

Midplane regions of circumstellar disks have a very low degree of ionization because of the intrinsic low temperature and strong shielding of the ionizing stellar radiation and cosmic-ray fluxes by the overlying disk layers. As a result, dust grains in the shielded layer are predominantly neutral, and their dipole moments are intrinsic and not due to an asymmetric charge distribution. Following DL98, we assume very small dust grains to be composed of randomly oriented chemical substructures, so that the total intrinsic dipole moment of the grain scales with the number of atoms in the grain N as

$$d \approx N^{1/2} d_0. \quad (3)$$

Based on the available laboratory data on the dipole moments of the PAH-like particles, DL98 have chosen $d_0 = 0.4 \text{ D}$ in their study, and we adopt this estimate as well.

The power emitted by a grain of radius a spinning at frequency ω is given by

$$P(a, \omega) = \frac{4}{9} \frac{d^2(a)\omega^4}{c^3} = \frac{16\pi}{27} \frac{d_0^2 \omega^4}{c^3} \frac{\rho a^3}{\mu_d}, \quad (4)$$

where ρ is the bulk density of grain material and μ_d is the mean mass of grain atoms ($\mu_d \approx 9.25 \text{ amu}$ for C:H = 3:1 carbonaceous material typical for PAHs). In deriving equation (4), we assumed that grains are spherical [so that $d^2(a) = d_0^2 (4\pi\rho a^3)/(3\mu_d)$] and that their dipole moments are randomly oriented with respect to their rotational axes.

To calculate the spectrum of the dipole emission of spinning grains, we also need to know the size distribution of nanoscale dust particles. Contrary to the expectation of small-dust depletion⁴ in circumstellar disks, recent observations of PAH features in Herbig Ae/Be disks suggest that very small grains may actually be more abundant in these systems than in the ISM (Habart et al. 2004). By analogy with DL98, we use the functional form for the grain size distribution

$$\frac{1}{n_{\text{H}}} \frac{dn}{da} = A_{\text{MRN}} a^{-3.5} + \frac{B}{a} \exp\left\{-\frac{1}{2} \left[\frac{\ln(a/a_0)}{\sigma}\right]^2\right\}, \quad (5)$$

where $A_{\text{MRN}} = 6.9 \times 10^{-26} \text{ cm}^{2.5}$ (Draine & Lee 1984) and B are constants, a_0 is the typical size of very small carbonaceous grains, and σ is the width of their lognormal distribution. The

⁴ DL98 assumed that in dense interstellar clouds PAHs are depleted by a factor of 5.

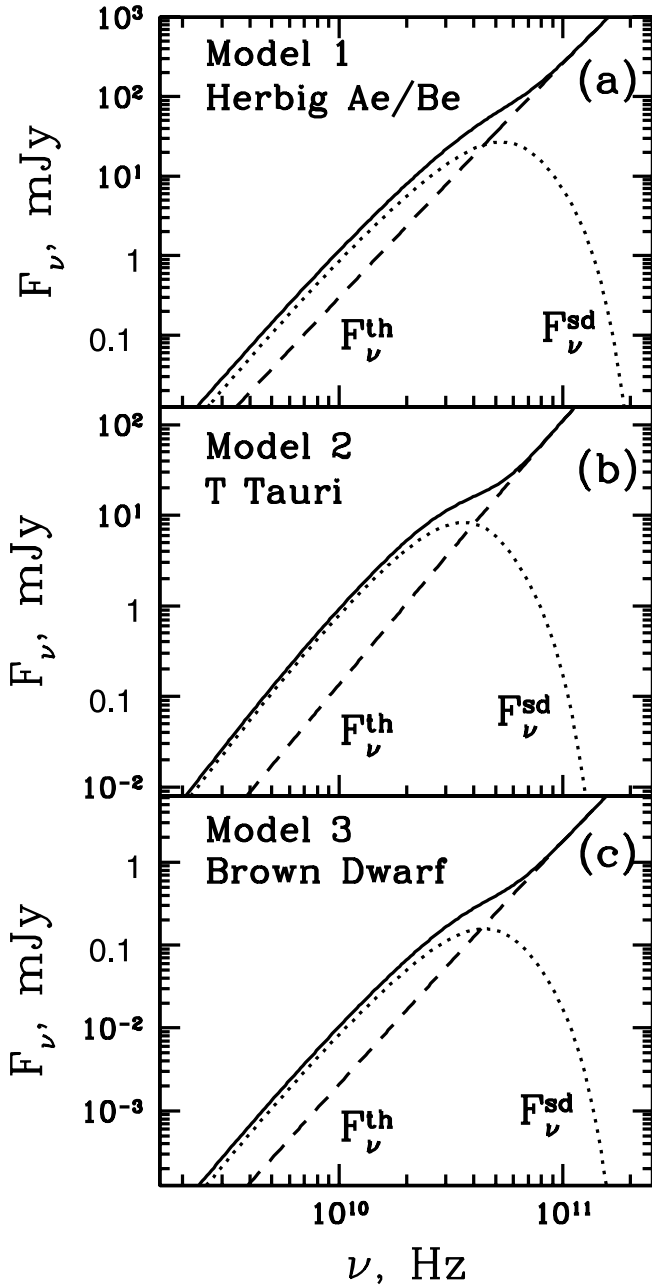


FIG. 1.—Spectrum of the microwave disk emission for systems described by models (a) 1, (b) 2, (c) and 3 placed 100 pc away from us. The Rayleigh-Jeans tail of the thermal disk emission (*dashed line*), the contribution of the spinning dust emission (*dotted line*), and their sum (*solid line*) are displayed. Thermal emission is calculated for the dust emissivity index $\beta = 1$ and behaves as $F_{\nu}^{\text{th}} \propto \nu^3$ (see text for other parameters). At radio wavelengths the spinning dust emission exceeds the thermal disk emission by $F_{\nu}^{\text{sd}}/F_{\nu}^{\text{th}}$ of (a) ≈ 3 , (b) ≈ 6 , and (c) ≈ 4 .

first term is a conventional MRN contribution, while the second accounts for very small grains. The coefficient B is chosen in such a way that the fraction of C locked up in very small grains (with respect to the total abundance $C/H = 4 \times 10^{-4}$) is f_C . Our baseline model uses $f_C = 0.05$ (close to the ISM value), $a_0 = 3 \text{ \AA}$, and $\sigma = 0.5$; this distribution extends down to a minimum size $a_{\min} = 3.5 \text{ \AA}$.

2.3. Grain Spin Rates

Rotation rates of small dust grains are in general governed by a combination of physical processes: collisions of grains with neutral molecules, Coulomb interactions with charged species,

TABLE 1
LIST OF MODELS USED FOR CALCULATION OF THE SPINNING DUST EMISSION

| Model | M_* (M_{\odot}) | R_* (R_{\odot}) | T_* (K) | R_{in} (AU) | R_{out} (AU) | Σ_1 (g cm^{-2}) | Object |
|--------|--------------------------|--------------------------|--------------|-------------------------|--------------------------|--------------------------------------|--------------|
| 1..... | 2 | 2 | 10000 | 1 | 300 | 1000 | Herbig Ae/Be |
| 2..... | 0.5 | 2 | 4000 | 0.1 | 300 | 1000 | T Tauri |
| 3..... | 0.1 | 1.3 | 2600 | 0.033 | 30 | 100 | Brown dwarf |

infrared and electric dipole emission, etc. (DL98). Since here we are mainly interested in obtaining a reasonable estimate of the importance of the spinning dust emission in disks, we assume that grain rotation is determined by thermal equilibrium.

This assumption is reasonable in the midplane region of the circumstellar disk because of the high gas density and very low ionization fraction there. Consequently, interactions of predominantly neutral dust grains with extremely rare charged particles (plasma drag/excitation and rotational excitation by ion collisions, which are often the most important determinants of grain spin rates in the ISM; see the case of molecular cloud environment in DL98) are completely negligible in this part of disk. As a result, grain-neutral collisions bring particle spin rates into thermal equilibrium with the surrounding gas.⁵ This implies that grain spin rates have a Boltzmann distribution,

$$f_{\omega}(\omega) = 4\pi \left(\frac{3}{2\pi}\right)^{3/2} \frac{\omega^2}{\langle \omega^2 \rangle^{3/2}} \exp\left(-\frac{3}{2} \frac{\omega^2}{\langle \omega^2 \rangle}\right), \quad (6)$$

with the rms rotation rate $\langle \omega^2 \rangle^{1/2}$ given by

$$\langle \omega^2 \rangle^{1/2} = \left(\frac{3k_B T}{I}\right)^{1/2} \approx 3.5 \times 10^{10} T_2^{1/2} a_{-7}^{5/2} \text{ s}^{-1}, \quad (7)$$

where T_2 is the gas temperature normalized to 10^2 K , a_{-7} is the grain radius in units of 10^{-7} cm , and we take $\rho = 2 \text{ g cm}^{-3}$. For simplicity, we assume the grain shapes to be close to spherical, implying that their moment of inertia is $I = (8\pi/15)\rho a^5$, although very small particles, like PAHs, are likely to be sheetlike (see DL98 for more refined treatment).

Within the upper exposed layer grains may spin at significantly nonthermal rates (corresponding to temperatures higher than the midplane temperature), but the amount of mass contained in this layer is very small, meaning that its contribution to the total spinning dust emission can be neglected in the first approximation.

2.4. Spectrum of the Spinning Dust Emission

Combining equations (4), (5), and (6), we find the total spectrum of the spinning dust emission produced by the disk,

$$\begin{aligned} F_{\nu}^{\text{sd}} &= 2\pi \int_{a_{\min}}^{a_{\max}} da \frac{1}{n_H} \frac{dn}{da} \int_{R_{\text{in}}}^{R_{\text{out}}} \frac{\Sigma(r)r dr}{m_H} P(a, \omega) 2\pi f_{\omega}(\omega) \\ &= 8\pi^2 \left(\frac{8}{3\pi}\right)^{1/2} \frac{\omega^6}{m_H c^3} \int_{a_{\min}}^{a_{\max}} \frac{1}{n_H} \frac{dn}{da} d^2(a) da \\ &\quad \times \int_{R_{\text{in}}}^{R_{\text{out}}} \frac{\Sigma(r)r dr}{\langle \omega^2 \rangle^{3/2}} \exp\left(-\frac{3}{2} \frac{\omega^2}{\langle \omega^2 \rangle}\right), \end{aligned} \quad (8)$$

⁵ Infrared emission by grains is unlikely to strongly affect their spin rates because of low midplane temperatures.

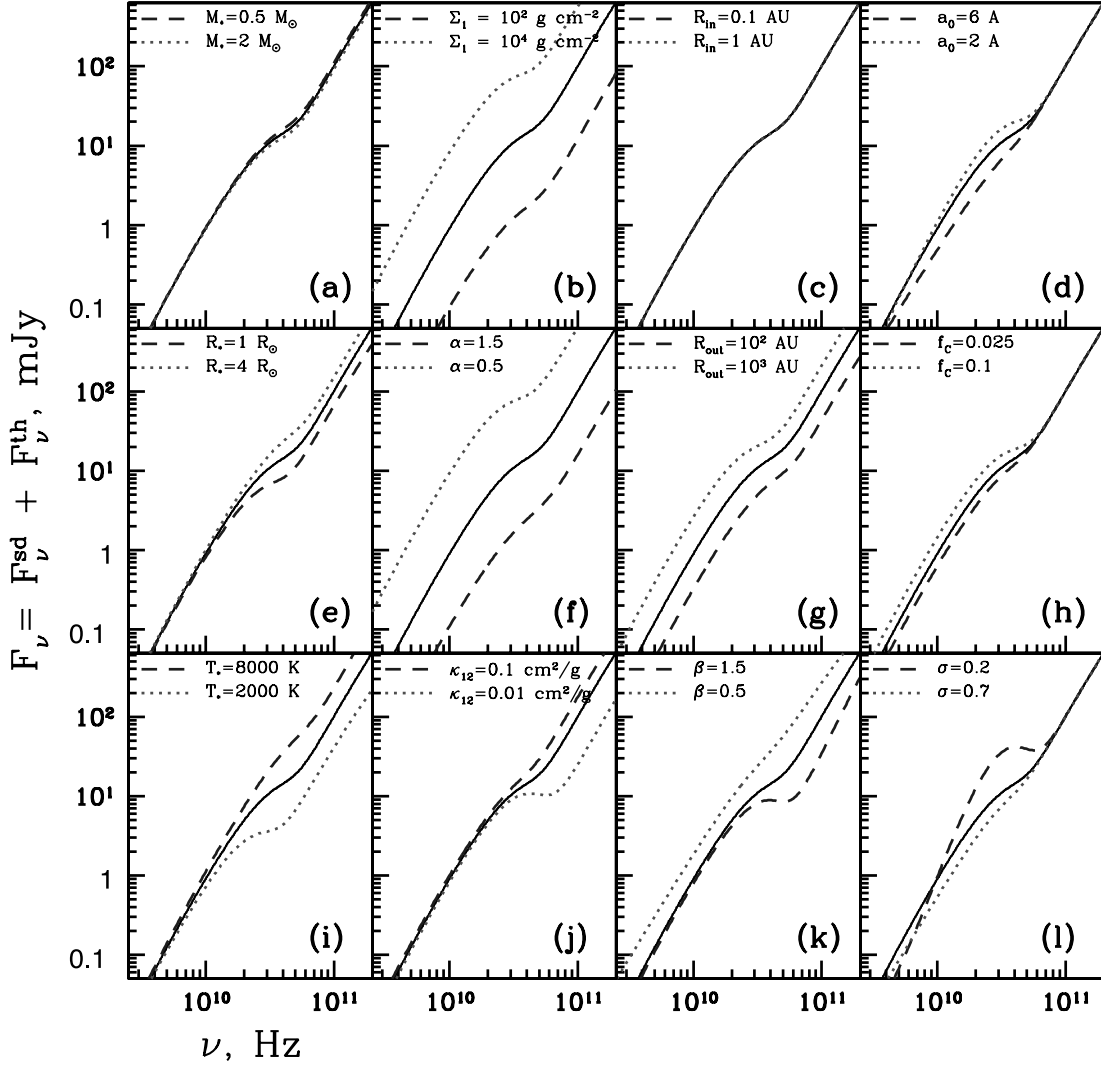


FIG. 2.—Evolution of the total disk spectrum (both thermal and spinning dust contributions included) caused by the variation of basic model parameters. Each window displays the results obtained by variation of a single parameter around the fiducial model described in the text. The parameter being varied and its values corresponding to different curves are indicated in each window. The solid curve always represents the spectrum of the fiducial model. [See the electronic edition of the *Journal* for a color version of this figure.]

where R_{in} and R_{out} are the inner and outer radii of the disk, $\langle \omega^2 \rangle$ is given by equation (7) as a function of $T(r)$, and the maximum grain size a_{max} is irrelevant for this calculation, since F_{ν}^{sd} is dominated by small grains.

For a simple case of a power-law temperature distribution $T(r) = T_0(r/R_*)^{-\gamma}$ and a dust population with a single characteristic size a , one finds that

$$F_{\nu}^{\text{sd}} \propto \nu^{3+2(\alpha-2)/\gamma}, \quad \nu_{\text{out}} \lesssim \nu \lesssim \nu_{\text{in}}, \quad (9)$$

where

$$\nu_{\text{out,in}} \sim \left(\frac{15 k_{\text{B}} T_0}{4\pi \rho a^5} \right)^{1/2} \left(\frac{R_{\text{out,in}}}{R_*} \right)^{-\gamma/2} \quad (10)$$

are the frequencies determining the extent of the power-law segment of F_{ν}^{sd} . The outer regions of irradiated disks can often be well characterized by $\gamma \approx 0.5$, yielding a slope of the power-

law section of F_{ν}^{sd} quite different from $2 + \beta$, which is a characteristic power-law index of the thermal disk emission,⁶

$$F_{\nu}^{\text{th}} = 2\pi \int_{R_{\text{in}}}^{R_{\text{out}}} B_{\nu}(T(r)) \psi_{\text{sh}}(T(r)) r dr \quad (11)$$

in the optically thin Rayleigh-Jeans regime (here B_{ν} is a Planck function and ψ_{sh} is defined in the Appendix; the power-law index of F_{ν}^{sd} is -1 for $\alpha = 1$ and 1 for $\alpha = 3/2$). As a result, one can hope to detect the spinning dust emission only at long wavelengths, where F_{ν}^{sd} may dominate over F_{ν}^{th} .

In Figure 1 we plot spectra of the spinning dust emission computed according to the prescription in equation (8) for circumstellar disks with different central objects at different evolutionary stages: a massive Herbig Ae/Be star, a solar-type T Tauri star, and a brown dwarf. Adopted parameters of these systems are listed in

⁶ This expression accounts for the fact that at long wavelengths F_{ν}^{th} is dominated by the cool shielded region and the contribution of the warm exposed layer is small.

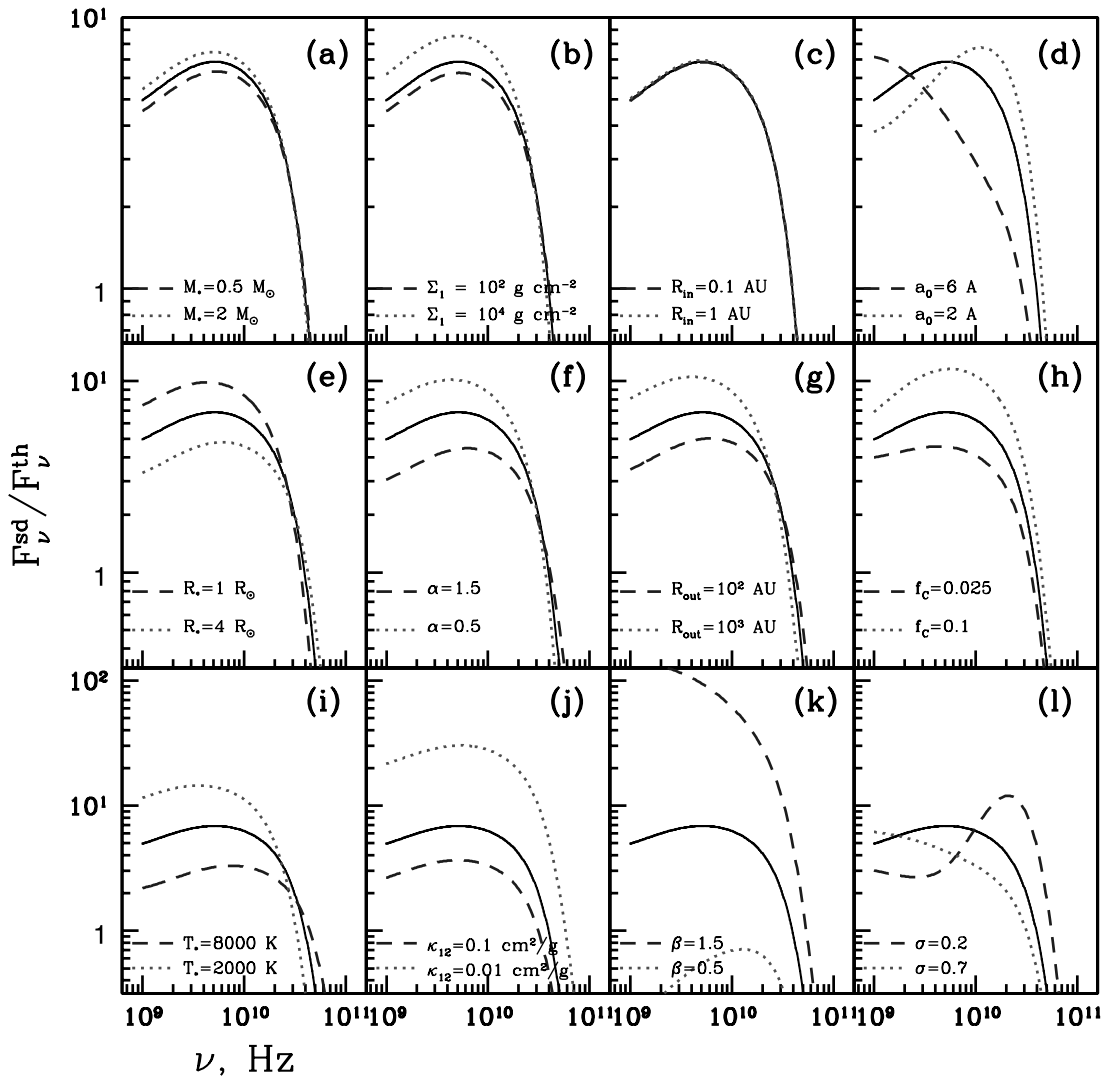


FIG. 3.—Evolution of the ratio $F_{\nu}^{\text{sd}}/F_{\nu}^{\text{th}}$ representing the strength of the spinning dust contribution relative to the thermal disk emission due to the variation of the model parameters with respect to the fiducial model. Notation is the same as in Fig. 2. [See the electronic edition of the Journal for a color version of this figure.]

Table 1 and are the same⁷ as in Dullemond & Natta (2003). In all models we use $\alpha = 1$, $\beta = 1$, and $\kappa_{12} = 0.05 \text{ cm}^2 \text{ g}^{-1}$ and adopt a baseline model of the grain size distribution in equation (5) with parameters listed in § 2.2. Disks are assumed to be located 100 pc away from us.

One can see that all three models exhibit significant excesses due to the spinning dust emission around 30 GHz. This component exceeds the thermal power-law contribution by a factor ranging from 3 to 6. Excess appears first at frequencies of about 50 GHz (the typical spin frequency of dust grains at low temperatures, see eq. [7]) and extends all the way to lower frequencies.

2.5. Sensitivity to Stellar and Disk Parameters

The appearance of the SED including the spinning dust component depends on a large number of stellar, dust, and disk parameters: M_* , R_* , Σ_1 , α , β , κ_{12} , etc. To test sensitivity to different parameters, we have varied them one at a time to see how the spectrum evolves with respect to a fixed fiducial model of the disk + star system. As a fiducial stellar model, we have adopted

⁷ Except the surface density normalization in the T Tauri model, which in our case is comparable to the minimum mass solar nebula value.

T Tauri model 2 but with $M_* = 1 M_{\odot}$ and $a_{\text{in}} = 0.3 \text{ AU}$ for the inner edge of the disk. The fiducial model also uses $\alpha = 1$, $\beta = 1$, and $\kappa_{12} = 0.05 \text{ cm}^2 \text{ g}^{-1}$. The parameters of the fiducial dust model are specified in § 2.2.

Figure 2 demonstrates how the total microwave spectrum of the disk $F_{\nu}^{\text{sd}} + F_{\nu}^{\text{th}}$ changes due to the parameter variation. Figure 3 shows the same, but for the ratio of fluxes $F_{\nu}^{\text{sd}}/F_{\nu}^{\text{th}}$. These plots demonstrate that the microwave spectrum is insensitive to both stellar mass M_* and R_{in} . The former appears only in the calculation of the radial temperature profile (see the Appendix), which depends on M_* only weakly. The inner radius of the disk does not play any role, since at centimeter wavelengths both the spinning dust emission and the thermal emission of the disk are dominated by the outer region, $r \sim R_{\text{out}}$. Variation of R_{out} changes mass of the emitting gas, which mainly affects the overall flux level (Fig. 2g) but also changes $F_{\nu}^{\text{sd}}/F_{\nu}^{\text{th}}$ somewhat (Fig. 3g). The same is true for the spectral sensitivity to Σ_1 and α ; variation of both parameters mainly affects the emitting dust mass, so the characteristic pattern of spectral evolution is similar to that caused by changing R_{out} (Figs. 2b and 2f and Figs. 3b and 3f). Spectral sensitivity to T_* and R_* is similar, as both parameters determine the stellar luminosity. Changing the parameters of the small-dust size distribution, a_0 , σ , and f_c , affects both the shape and

normalization of the spinning dust spectrum, leaving the thermal disk emission (dominated by large grains) unaffected.

Variations of κ_{12} do not affect the spinning dust emission but change the optical depth of the disk, which then affects F_ν^{th} (see Fig. 2*j*). As a result, for low enough opacity (e.g., $\kappa_{12} = 0.01 \text{ cm}^2 \text{ g}^{-1}$) spinning dust emission can dominate over the thermal disk emission by more than an order of magnitude at $\nu \lesssim 30 \text{ GHz}$ (see Fig. 3*j*). A similar effect is produced by the variation of the dust emissivity index β : it changes the thermal flux of the disk by orders of magnitude, since $F_\nu^{\text{th}} \propto \nu^{2+\beta}$ (see Figs. 2*k* and 3*k*).

The total power produced by the disk determines whether it can be detected in a flux-limited observation. However, even if such a detection is made, one can disentangle the spinning dust component from the thermal disk emission only if $F_\nu^{\text{sd}}/F_\nu^{\text{th}} \gtrsim 1$. Examination of Figure 3 demonstrates that this is most easily done for small κ_{12} and/or large β . Coagulation of dust particles in dense circumstellar disk environments generally tends to decrease β (sometimes below 1), which would hide the spinning dust emission bump in the thermal power-law component of the spectrum (see the curve for $\beta = 0.5$ in Fig. 2*k*). Thus, from the observational point of view the most favorable chances of detecting the spinning dust emission would be in systems having steep submillimeter slopes of the SED ($\beta \gtrsim 1$).

3. DISCUSSION

There is strong evidence for the presence of the anomalous microwave emission correlated with the thermal emission from interstellar dust in the data obtained by the CMB (cosmic microwave background) experiments (Kogut et al. 1996; Bennet et al. 2003) and by the recent Green Bank Galactic Plane Survey (Finkbeiner et al. 2004). It appears likely that this emission is due to the electric dipole emission of the spinning ISM dust grains (Draine & Lazarian 1998a; Finkbeiner 2004), although other explanations such as magnetic dipole emission caused by thermal fluctuations in the magnetization of interstellar grains (Draine & Lazarian 1999) or dust-correlated synchrotron emission (Bennet et al. 2003) are also possible. This motivates us to investigate the possibility of using spinning dust emission to study the small-dust population in protoplanetary disks.

Results presented in § 2 clearly demonstrate that in the case of protoplanetary disks, the spinning dust contribution to the microwave emission is substantial and often significantly exceeds the thermal dust emission at $\nu \lesssim 30\text{--}50 \text{ GHz}$, provided that the small-dust population integrated over the whole disk amounts to $\gtrsim 5\%$ of the total C content. Whether the spinning dust emission is detectable depends on the presence of other spectral contributions in the microwave band. These include free-free emission from the gas heated by the central star or by the nearby massive stars and synchrotron emission from jets and outflows, which accompany a large fraction of the young stellar objects. Spinning dust emission can be discriminated from these components based on its intrinsic bell-like spectral shape, since both free-free and synchrotron emission are characterized by power-law spectra. Power-law spectral tails at centimeter wavelengths extending sometimes for more than a decade in frequency have indeed been observed in some objects (Zapata et al. 2006; Eisner & Carpenter 2006), suggesting the contamination by free-free and synchrotron emission. Given broad enough frequency coverage in the radio, one can detect these power-law components at lower frequencies, extrapolate them to 10–50 GHz, and subtract from the total flux. Spinning dust emission will be present in the remaining flux, provided that it dominates over such power-law contaminants (its detection would be facilitated by its intrinsic

spectral shape). Note that because of the high stellar temperature, the contamination with free-free emission may be especially severe in Herbig Ae/Be systems, potentially allowing only the upper limits to be set on the flux due to the spinning dust.

Another way of deducing possible free-free contamination is to look for H α emission from the same object, since both components originate in the same hot gas. This would give a useful handle on the expected strength of the free-free flux at low frequencies and demonstrate a priori whether it can compete with the spinning dust emission in the microwave domain. The synchrotron contribution can be identified based on its polarization and the morphology of the synchrotron-emitting outflows (for which reasonable quality imaging would be required).

Provided that these difficulties can be successfully overcome, the potential detection (or nondetection) of the spinning dust emission can give us very interesting information on the small-dust population in the circumstellar disks. There is already strong evidence for the existence of such a population in disks around Herbig Ae/Be stars based on the detection of PAH emission features in the 6–12 μm band (van Kerckhoven et al. 2002; Schütz et al. 2005; Sloan et al. 2005; Habart et al. 2005) excited by the copious UV flux of the central star. The total observable mass of small dust particles producing near-IR emission features is very small, $M_s \sim 10^{23}\text{--}10^{24} \text{ g}$ (van Kerckhoven et al. 2002), but one has to remember that the favorable PAH excitation conditions exist only in the very thin outermost layers of the disk, where the stellar UV flux gets fully absorbed. As a result, emission in PAH bands shows only the very tip of the iceberg, as it traces an insignificant fraction of the total population of small dust. Most of the nanoparticles can be hidden from stellar UV near the disk midplane (provided that they are homogeneously distributed) and constitute substantial fraction of the total dust population (see Habart et al. 2004). As the spinning dust emission is contributed by all small dust particles (the disk is optically thin at microwave frequencies), its detection would give us a very useful probe of the total mass in nanoparticles. Combined with the model for the disk structure, the comparison of the near-IR PAH observations and the spinning dust emission would provide a very good consistency check for the two probes of the small-dust population.

A nondetection of the spinning dust emission in Herbig Ae/Be systems with observed near-IR PAH bands may suggest that either (1) PAH formation is catalyzed by stellar UV in the uppermost disk layer, and they are rapidly destroyed in its interior (which may seem rather exotic), or (2) large grains have strongly settled toward the disk midplane. The latter possibility is worth exploring in more detail. The column density of disk material exposed to radiation exciting PAH emission is $\approx \gamma/\kappa^{\text{ex}}$, where the flaring angle $\gamma \sim 0.1$ is a weak function of the distance from the star. The opacity κ^{ex} at the wavelengths where PAH excitation is most effective ($\lambda \sim 0.2 \mu\text{m}$) is contributed both by large grains and nanoparticles: $\kappa^{\text{ex}} = \kappa_b^{\text{ex}} f_b + \kappa_s^{\text{ex}} f_s$, where $\kappa_b^{\text{ex}} \sim 4 \times 10^4 \text{ cm}^2 \text{ g}^{-1}$ (Draine 2003) and $\kappa_s^{\text{ex}} \sim 3 \times 10^5 \text{ cm}^2 \text{ g}^{-1}$ (Li & Draine 2002) are the opacities *per unit dust mass* of big grains and nanoparticles at $\lambda \sim 0.2 \mu\text{m}$, and f_b and f_s are the abundances of large grains and nanoparticles relative to H by mass. The mass of small dust visible in PAH emission integrated over the whole disk (within r_{PAH} from the star) can then be found as

$$M_s \approx \frac{\gamma f_s \pi r_{\text{PAH}}^2}{\kappa_b^{\text{ex}} f_b + \kappa_s^{\text{ex}} f_s} \approx 6 \times 10^{23} \text{ g} \left(\frac{r_{\text{PAH}}}{50 \text{ AU}} \right)^2 \left(\frac{\gamma}{0.1} \right) \left(1 + \frac{\kappa_b^{\text{ex}} f_b}{\kappa_s^{\text{ex}} f_s} \right)^{-1}, \quad (12)$$

which is in good agreement with the observed mass of PAHs producing near-IR emission in Herbig Ae/Be disks (van Kerckhoven et al. 2002). Our estimate of r_{PAH} is based on recent high angular resolution observations of PAH emission in Herbig Ae/Be systems (Habart et al. 2005) demonstrating that about 50% of integrated PAH emission comes from within 30 AU.

In the ISM one expects $f_b \sim 0.01$ and $f_s \approx 2.5 \times 10^{-4}$ (corresponding to $f_C = 0.05$ and $C/H = 4 \times 10^{-4}$), so that the expression in parentheses in equation (12) is ≈ 6 . In protoplanetary disks f_b may go down as a result of sedimentation of big grains, while f_s may decrease because of coagulation of nanoparticles or increase because of fragmentation of big grains. Sedimentation of nanoparticles during the lifetime of a protoplanetary disk is negligible. Habart et al. (2004) modeled PAH emission from Herbig Ae/Be disks and found good agreement with the data for $f_s = 6 \times 10^{-4}$, assuming that big grains are undepleted from the uppermost disk layers ($f_b \sim 0.01$). However, equation (12) clearly demonstrates that what disk surface PAH emission really probes is the *ratio* f_b/f_s rather than f_b or f_s separately. Thus, the Habart et al. (2004) measurement really implies only that $f_b/f_s \approx 16$. Any depletion of large grains caused by their sedimentation toward the midplane immediately translates into values of f_s smaller than that derived by Habart et al. (2004). Thus, for a given intensity of near-IR PAH emission, sedimentation of big grains lowers f_s and reduces the chances of detecting microwave spinning dust emission.

On the other hand, it is likely that sedimentation cannot deplete big grains in surface layers of Herbig Ae/Be disks exhibiting strong PAH emission dramatically, since these disks have *flared* geometry as inferred from their SEDs (Habart et al. 2004)—this would not be possible if strong sedimentation had occurred. In fact, one may invert the problem and use observations of the spinning dust emission to learn about the dust sedimentation in disks: microwave emission would directly yield the value of f_s (very small dust grains are expected to be well mixed), while near-IR PAH emission provides a sensitive probe of f_b/f_s in the disk surface as long as $f_b/f_s \gtrsim \kappa_s^{\text{ex}}/\kappa_b^{\text{ex}} \approx 10$. A combination of these methods determines the abundance of big grains f_b in the surface layers of the disk, which, compared to the ISM value of f_b , measures the degree of dust settling.

With only a few exceptions (e.g., Geers et al. 2005), mid-IR PAH emission has not been detected in disks around T Tauri stars or brown dwarfs. This fact is consistent with the lack of strong UV flux in these objects, which is necessary for efficient excitation of the PAH features (although see Li & Draine 2002; Smith et al. 2004 for a different opinion), and should not be immediately interpreted as evidence for the absence of the nanoparticle dust component in these systems. Because of the lack of PAH emission, the microwave emission of spinning dust may be the only⁸ way in which the small dust could be probed in T Tauri and brown dwarf disks.

Unlike the mid-IR PAH features, spinning dust emission reveals the whole nanoparticle dust population of the disk, which is important in many respects. Small particles affect the ionization balance within the disk, since they dominate the dust surface area and are very efficient at immobilization of free charges. This works against the operation of the magnetorotational instability in protoplanetary disks (Fleming & Stone 2003), which, in turn, affects the sizes and positions of the so-called “dead zones” of quiescent nonturbulent material (Gammie 1996), with potential consequences for planet formation (Matsumura & Pudritz 2005,

2006). Small grains also affect heating of gas in the upper rarefied disk layers due to the higher yield of electrons from PAHs (Kamp & Dullemond 2004).

The very existence of substantial amounts of nanoparticles is very interesting from the evolutionary point of view, since dust grains are expected to grow as disks age. Recent discoveries of PAHs in Herbig Ae/Be disks in amounts exceeding those in the ISM (Habart et al. 2005) are at odds with this expectation but may be in line with the recent work of Dullemond & Dominik (2005), who found that dust fragmentation, in addition to coagulation, has to be an important ingredient of the dust evolution in protoplanetary disks. It may also be the case that the material properties of small and large grains (e.g., sticking coefficient) are completely different, leading to divergent evolutionary paths of the two extremes of the grain size distribution. Detection of the spinning dust emission from circumstellar disks may shed enough light on the properties of the small-dust population to resolve this puzzle.

The calculations presented in § 2 were intended to provide us with a rough idea for the importance of the spinning dust emission, and as such they neglected a number of details. Among them are the realistic distribution of shapes of the nanoscale dust particles, emission of spinning dust in the exposed layer associated with the nonthermal grain rotation rates, possible ionization of small dust particles in this layer, and so on. In this study we have also neglected the possible contribution of magnetic dipole emission of magnetized dust grains (Draine & Lazarian 1999) at microwave frequencies, which can be important⁹ in protoplanetary disks. In the future observational demands may warrant a more refined study including all these details.

4. SUMMARY

We have studied the electric dipole emission produced by spinning dust grains of very small size (several to tens of nm) in circumstellar disks. At the temperatures characteristic for these environments spinning grains emit in the microwave range, with the peak of the emission occurring at ~ 30 – 50 GHz. For typical parameters of disks around Herbig Ae/Be stars, T Tauri stars, and brown dwarfs we find spinning dust emission to dominate over the thermal disk emission by a factor of at least several at $\nu \lesssim 50$ GHz (if nanoparticles contain $\gtrsim 5\%$ of the total C abundance). We have studied the sensitivity of this emission component to various stellar, disk, and dust parameters and found it to be strongest for variations of the total dust opacity, both normalization of κ_ν , and the slope of its frequency dependence. Provided that the contamination of the spinning dust emission by the free-free and/or synchrotron emission can be mitigated, the best chances of detecting this emission component should be in systems with steep submillimeter spectral indices minimizing the contribution of the thermal disk emission. Detection (or nondetection) of the spinning dust emission will provide important information about the existence, properties, and origin of the nanoscale dust particles in circumstellar disks.

Useful comments on the manuscript by Aigen Li and Bruce Draine are greatly appreciated. R. R. R. thankfully acknowledges the support of this work by the Canada Research Chairs program and Connaught Foundation.

⁸ The contribution of very small particles to IR opacity is degenerate with that of large grains.

⁹ This emission can complicate the interpretation of microwave emission as being produced solely by electric dipole emission of spinning grains. However, one may hope to use the intrinsic spectral shape of the magnetic dipole emission (which is somewhat different from that of electric dipole emission) to disentangle its contribution to the microwave emission.

APPENDIX

RADIAL TEMPERATURE PROFILE IN THE DISK MIDPLANE

Thermal balance of the shielded region is set by $(\delta/4)T_*^4(R_*/a)^2\psi_{\text{ex}} = T_{\text{sh}}^4\psi_{\text{sh}}$, where T_{sh} and T_{ex} are the characteristic temperatures of the shielded and exposed regions, respectively, and ψ_{ex} and ψ_{sh} are the fractions of the radiative flux with blackbody temperatures T_{ex} and T_{sh} absorbed by the disk. In the optically thick case $\psi_{\text{ex,sh}} = 1$, while in the optically thin regime $\psi_{\text{ex,sh}} = \Sigma\kappa_{\text{P}}(T_{\text{ex,sh}})$. The flaring angle $\delta \equiv d(H_1/a)/d \ln a$ is determined by the height of the disk surface $H_1 \approx \lambda c_s(T_{\text{sh}})/\Omega$, where c_s is the gas sound speed and Ω is the angular frequency of the disk. The factor $\lambda \sim 1$ is roughly constant throughout the disk, and we set $\lambda = 3$ in this study. Power-law scaling of κ_{ν} implied by equation (2) results in the following expression for the low temperature Planck opacity:

$$\kappa_{\text{P}}(T) = \kappa_* \left(\frac{T}{T_*} \right)^\beta, \quad \kappa_* = \frac{15}{\pi^4} \frac{\kappa_{12}}{(10^{12} \text{ Hz})^\beta} \left(\frac{k_{\text{B}}}{h} \right)^\beta \int_0^\infty \frac{x^{3+\beta} dx}{e^x - 1}, \quad (\text{A1})$$

where β is the same as the power-law index in equation (2). The opacity dependence given by equation (A1) applies to the emission of both the disk interior and the exposed layer, but not to the stellar radiation, so that $\kappa_{\text{P}}(T_*)$ is significantly different from κ_* . In our case $\kappa_{\text{P}}(T_*)$ is calculated for a population of small $0.1 \mu\text{m}$ dust grains (Draine & Lee 1984; Dullemond & Natta 2003). Using equation (A1), one finds that

$$T_{\text{ex}}(r) = T_* \left[\frac{\kappa_{\text{P}}(T_*)}{4\kappa_*} \right]^{1/(4+\beta)} \left(\frac{R_*}{r} \right)^{2/(4+\beta)}. \quad (\text{A2})$$

This information allows one to derive the temperature profile in the shielded layer in different parts of the disk. The inner disk is optically thick to radiation at both T_{ex} and T_{sh} , which results in

$$T_{\text{sh}}(r) = T_* \left(\frac{\lambda}{14} \frac{h_*}{R_*} \right)^{2/7} \left(\frac{r}{R_*} \right)^{-3/7}. \quad (\text{A3})$$

In the intermediate region the disk is optically thin to the radiation of its interior [$\psi_{\text{sh}} = \Sigma\kappa_{\text{P}}(T_{\text{sh}}) < 1$] while still optically thick to the reprocessed emission of the exposed layer ($\psi_{\text{ex}} = 1$). As a result,

$$T_{\text{sh}}(r) = T_* \left[\frac{2 + \alpha + \beta}{4(7 + 2\beta)} \frac{\lambda}{\kappa_* \Sigma_*} \frac{h_*}{R_*} \right]^{2/(7+2\beta)} \left(\frac{r}{R_*} \right)^{(2\alpha-3)/(7+2\beta)}, \quad (\text{A4})$$

where $\Sigma_* = \Sigma(R_*)$ is a value of Σ obtained by extrapolation of equation (1) to $r = R_*$. Finally, in the outer disk, which is optically thin to the radiation at both T_{ex} and T_{sh} , one finds

$$T_{\text{sh}}(r) = T_* \left[\frac{\beta^2 + 4\beta + 8}{4(4 + \beta)(7 + 2\beta)} \lambda \frac{h_*}{R_*} \right]^{2/(7+2\beta)} \left[\frac{\kappa_{\text{P}}(T_*)}{4\kappa_*} \right]^{2\beta/[(4+\beta)(7+2\beta)]} \left(\frac{r}{R_*} \right)^{-(7\beta+12)/[(4+\beta)(7+2\beta)]}. \quad (\text{A5})$$

Transition between the inner and intermediate regions occurs at

$$a_1 \approx R_* (\kappa_* \Sigma_*)^{7/(7\alpha+3\beta)} \left(\frac{\lambda}{14} \frac{h_*}{R_*} \right)^{2\beta/(7\alpha+3\beta)} \quad (\text{A6})$$

and between the intermediate and outer regions at

$$a_2 \approx R_* (\kappa_* \Sigma_*)^{(4+\beta)/[2\beta+\alpha(4+\beta)]} \left[\frac{\kappa_{\text{P}}(T_*)}{4\kappa_*} \right]^{\beta/[2\beta+\alpha(4+\beta)]}. \quad (\text{A7})$$

In a particular case of $\alpha = 3/2$ and $\beta = 1$, our results agree with Chiang & Goldreich (1997). The profile of $T_{\text{sh}}(r)$ used in § 2 is found by extrapolation between expressions in equations (A3)–(A5).

REFERENCES

- Acke, B., & van den Ancker, M. E. 2004, *A&A*, 426, 151
Acke, B., van den Ancker, M. E., Dullemond, C. P., van Boekel, R., & Waters, L. B. F. M. 2004, *A&A*, 422, 621
Apai, D., et al. 2005, *Science*, 310, 834
Beckwith, S. V. W., Sargent, A. I., Chini, R. S., & Guesten, R. 1990, *AJ*, 99, 924
Bennett, C. L., et al. 2003, *ApJS*, 148, 97
Boulanger, F., & Pérault, M. 1988, *ApJ*, 330, 964
Chiang, E. I., & Goldreich, P. 1997, *ApJ*, 490, 368
Draine, B. T. 2003, *ARA&A*, 41, 241
———. 2006, *ApJ*, 636, 1114
Draine, B. T., & Anderson, N. 1985, *ApJ*, 292, 494
Draine, B. T., & Lazarian, A. 1998a, *ApJ*, 494, L19
———. 1998b, *ApJ*, 508, 157 (DL98)
———. 1999, *ApJ*, 512, 740
Draine, B. T., & Lee, H. M. 1984, *ApJ*, 285, 89
Dullemond, C. P., & Dominik, C. 2005, *A&A*, 434, 971

- Dullemond, C. P., & Natta, A. 2003, *A&A*, 405, 597
Eisner, J. A., & Carpenter, J. M. 2006, *ApJ*, 641, 1162
Ferrara, A., & Dettmar, R.-J. 1994, *ApJ*, 427, 155
Finkbeiner, D. P. 2004, *ApJ*, 614, 186
Finkbeiner, D. P., Davis, M., & Schlegel, D. J. 1999, *ApJ*, 524, 867
Finkbeiner, D. P., Langston, G. I., & Minter, A. H. 2004, *ApJ*, 617, 350
Fleming, T., & Stone, J. M. 2003, *ApJ*, 585, 908
Gammie, C. F. 1996, *ApJ*, 457, 355
Geers, V. C., et al. 2005, in *Protostars and Planets V Abstract Vol. (LPI Contrib. 1286; Houston: LPI)*, 8409
Habart, E., Natta, A., & Krügel, E. 2004, *A&A*, 427, 179
Habart, E., Natta, A., Testi, L., & Carbillet, M. 2006, *A&A*, 449, 1067
Kamp, I., & Dullemond, C. P. 2004, *ApJ*, 615, 991
Kitamura, Y., Momose, M., Yokogawa, S., Kawabe, R., Tamura, M., & Ida, S. 2002, *ApJ*, 581, 357
Kogut, A., Banday, A. J., Bennett, C. L., Gorski, K. M., Hinshaw, G., & Reach, W. T. 1996, *ApJ*, 460, 1
Kramer, C., et al. 1998, *A&A*, 329, L33
Leger, A., & Puget, J. L. 1984, *A&A*, 137, L5
Li, A., & Draine, B. T. 2002, *ApJ*, 572, 232
Mathis, J. S., Rumpl, W., & Nordsieck, K. H. 1977, *ApJ*, 217, 425
Matsumura, S., & Pudritz, R. E. 2005, *ApJ*, 618, L137
———. 2006, *MNRAS*, 365, 572
Meeus, G., et al. 2001, *A&A*, 365, 476
Natta, A., Testi, L., Neri, R., Shepherd, D. S., & Wilner, D. J. 2004, *A&A*, 416, 179
Schütz, O., Meeus, G., & Sterzik, M. F. 2005, *A&A*, 431, 165
Sloan, G. C., et al. 2005, *ApJ*, 632, 956
Smith, T. L., Clayton, G. C., & Valencic, L. 2004, *AJ*, 128, 357
Testi, L., Natta, A., Shepherd, D. S., & Wilner, D. J. 2003, *A&A*, 403, 323
van Boekel, R., Min, M., Waters, L. B. F. M., de Koter, A., Dominik, C., van den Ancker, M. E., & Bouwman, J. 2005, *A&A*, 437, 189
van Kerckhoven, C., Tielens, A. G. G. M., & Waelkens, C. 2002, *A&A*, 384, 568
Zapata, L. A., Rodríguez, L. F., Ho, P. T. P., Beuther, H., & Zhang, Q. 2006, *AJ*, 131, 939